Partial-ring PET Image Correction using Implicit Neural Representation Learning

Shubhangi Makkar[1,2], Siqi Ye[3], Marina Béguin[2], Günther Dissertori[2], Jan Hrbacek[1], Antony Lomax[1,2], Keegan McNamara[1,2], Christian Ritzer[2], Damien C. Weber[1,4,5], Lei Xing[3], and Carla Winterhalter[1]

[1]Center for Proton Therapy, PSI, Switzerland
[2]Department of Physics, ETH Zürich, Switzerland
[3]Department of Radiation Oncology, Stanford University, Palo Alto, California, USA
[4]Radiation Oncology Department of the University Hospital of Zurich, Switzerland
[5]Department of Radiation Oncology, Inselspital, Bern University Hospital, University of Bern, Switzerland

Abstract This work introduces a deep learning-based approach to enhance image quality in partial-ring PET scanners, which often suffer from significant artifacts due to incomplete angular field of view. Our method utilizes implicit neural representation (INR) learning with coordinate-based multilayer perceptrons (MLPs) featuring sinusoidal activations. These MLPs parameterize partial-ring PET images, training the patient-specific network to predict fully sampled images from partially sampled ones. This approach was validated using twenty digital brain phantoms, Monte Carlo simulated Derenzo phantom, and experimentally acquired hot rod phantom data from the partial-ring PETITION PET scanner. The results show that the INR learning method significantly improves image quality, achieving a PSNR above 30dB and SSIM over 0.95 for all cases. This method presents a promising solution for enhancing PET images from partial-ring scanners.

1 Introduction

Positron Emission Tomography (PET) plays an important role in functional imaging. Traditional PET systems rely on detectors arranged in a ring configuration [1, 2] to capture comprehensive imaging data across all angular views. However, the emergence of partial-ring PET systems has introduced both economical and practical advantages, particularly in specialized applications such as locoregional imaging [3] or online heavy-ion therapy verification [4]. Despite these benefits, partial-ring configurations inherently suffer from incomplete data acquisition, leading to significant image artifacts and reduced image quality.

Previously, model-based techniques have been employed to correct limited-angle PET images. For instance, sinogram completion using interpolation prior to reconstruction is an approach [5]. Another approach is the use of compressed sensing [6], which leverages the sparsity of data in a transform domain. Applying regularization constraints such as total variation [7] further helps in enforcing smoothness, thereby helping in artefact reduction. However, these model-based approaches have limitations, particularly when it comes to parameter optimization for regularization and computation times. To address these limitations, recent advances in deep learning (DL) and medical imaging have opened new pathways. The concept of implicit neural representation (INR) [8] presents a promising approach to obtain high-fidelity images from incomplete data sets [9]. The potential of deep learning, particularly in the context of INR learning, offers an innovative approach to correct and enhance PET images acquired from partial-ring systems. Unlike conventional DL approaches that depend on large labeled datasets, INR's ability to train unsupervised with sparse data makes it ideal for enhancing image quality in partial-ring PET systems. Here, we propose a framework that uses INR learning to effectively correct partial-ring PET images, particularly focusing on the developed partial-ring PETITION (PET for InTensive care units and Innovative protON therapy) scanner's design for proton therapy [10].

2 Materials and Methods

2.1 INR-based PET Image Correction

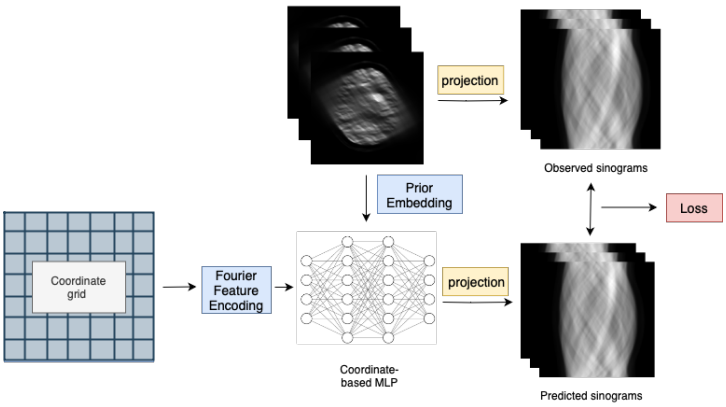

Figure 1: Network architecture for partial-ring PET image correction.

INR learning involves representing images using a neural network. We used a coordinate-based multi-layer perceptron (MLP) [8], $M(\theta)$ that transforms pixel coordinates $\{\mathbf{c}_i\}$ into their corresponding intensities.Our model consists of an MLP with 8 fully connected lay-

ers, 256 neurons each, employing sinusoidal activation functions. For efficient high-frequency signal representation, we used Fourier feature encoding, given by $F(\mathbf{c}_i) = [\cos(2\pi\mathbf{B}\mathbf{c}_i), \sin(2\pi\mathbf{B}\mathbf{c}_i)]^T$. The matrix $\mathbf{B}$, drawn from a Gaussian distribution with $\sigma = 4$ controls the frequency range. Inspired by a previous work that initialises the INR network parameters by pre-initialising the network with a prior image [9], we pre-trained the network with the uncorrected PET image from the limited-angle scan, which is the only accessible PET image of the scanned object in the real clinical scenario.

The PET reconstruction problem is often described as

$$\hat{\mathbf{x}} = \underset{\mathbf{x}}{\operatorname{argmin}} \|\mathbf{A}\mathbf{x} - \mathbf{y}\|_2^2, \tag{1}$$

where $\mathbf{x}$ is the reconstructed image, $\mathbf{y}$ is the measured data, and $\mathbf{A}$ is the forward model encapsulating the imaging physics.

With the INR learning, we parameterised the image $\mathbf{x}$ by the INR network, i.e., $\mathbf{x} = \mathcal{M}(\theta)$. The corresponding training loss function is therefore designed as

$$\hat{\theta} = \underset{\theta}{\operatorname{argmin}} \|\mathbf{A}\mathcal{M}(\hat{\theta}) - \mathbf{y}\|_2^2. \tag{2}$$

Once trained, the recovered image $\hat{\mathbf{x}}$ is inferred by $\hat{\mathbf{x}} = \mathcal{M}(\hat{\theta})$. The network architecture is depicted in Figure 1.

2.2 Datasets

Three distinct datasets employed for evaluation of our network are as follows:

- **MRI-based Brain Phantoms:** Twenty brain phantoms were sourced from BrainWeb [11, 12], and were adjusted to the PETITION scanner's resolution. Grey to white matter ratio was set at $4:1$, mimicking ^{18}F[FDG] PET and a hyperintense lesion was added onto each phantom. The geometry and the angular field of view of the PETITION PET scanner [10] was replicated.

- **Monte Carlo Simulation:** A Derenzo phantom with spheres of diameter 2.0, 2.2, 2.6, 3.2, 4.0 and 5.0 mm was simulated in GATE(v9.0) [13], where each sphere was uniformly filled with ^{18}F. The total simulated activity was 19 MBq with the acquisition time being 1800 seconds.

- **Real-Data Acquisition:** Utilizing a hot-rod phantom with uniform ^{18}F distribution, data was experimentally acquired with the PETITION PET scanner to reflect a realistic scenario of the physical effects.

2.3 Model Training

Model training was performed on a NVIDIA GV100GL GPU using PyTorch with the Adam optimiser. The model's performance was assessed using mean squared error (MSE), peak signal-to-noise ratio (PSNR), structural similarity index measure (SSIM) for different datasets in comparison to the ground-truth image that would have been obtained with a full-ring PET scanner. For the digital brain phantom dataset, we also compared the INR model with the widely used 2D U-Net [14]. Unlike the INR, the U-Net, being a data-dependent model, required division of the data into training, testing, and validation sets. Of the twenty brain phantoms, fifteen were allocated for training, four for testing, and one for validation. For the Derenzo phantom, peak-to-valley (PTV) ratios were computed for line profiles generated through different sphere diameters to assess the quantitative performance of the model. PTV ratio was calculated as the average intensity ratio of the uptake and no uptake region for each sphere.

3 Results

3.1 Digital Brain Phantoms

Figure 2 presents a comparison of various images for a slice of one of the brain phantoms. Quantitative comparison shows that the input partial-ring image lacks clarity (low PSNR and SSIM) and cannot reconstruct the lesion effectively. The U-Net and INR yielded similar SSIM and PSNR values, but INR-based correction outperformed U-Net in lesion reconstruction visually (figure 2) along with the required training times (15 minutes vs. 2 hours for U-Net).

3.2 MC Simulated Derenzo Phantom

Figure 3 displays the INR-corrected Derenzo phantom image, showing visually clear distinction between uptake and no-uptake regions. With prior initialization, INR achieves a PSNR of 31.73dB and an MSE error of 4×10^{-4}. Without prior initialization, it achieves a PSNR of 27.95dB and an MSE error of 1×10^{-3}. INR also exhibits higher SSIM values (0.95 with prior, 0.82 without) compared to the ground truth full-ring image. Quantitative analysis using PTV ratios (Figure 4) further validates the superior performance of INR, particularly when initialized with a prior. PTV ratios for the 2mm spheres are not indicated as this is beyond the resolution capabilities of the PETITION scanner.

3.3 Measured Hot-Rod Phantom

Visual comparison in Figure 5 demonstrates the improved image quality of the INR-reconstructed image

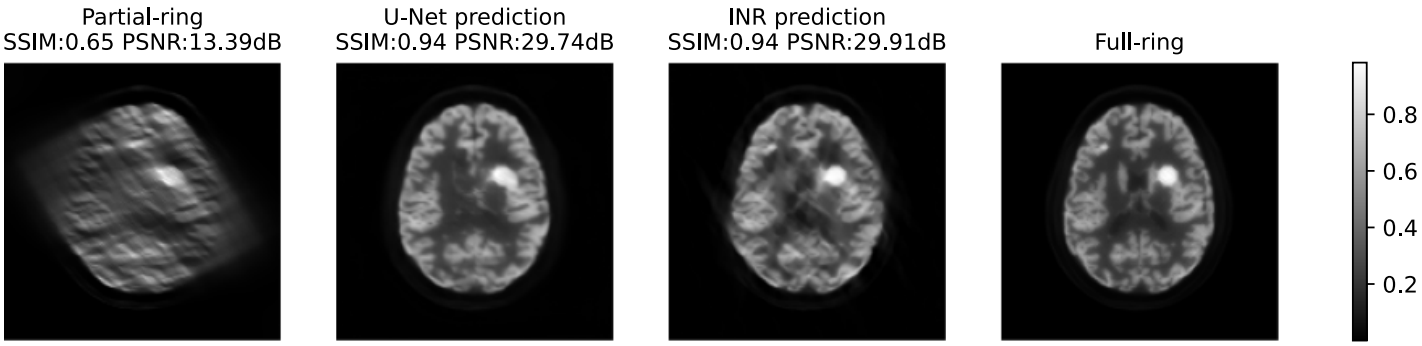

Figure 2: The central slice of a digital brain phantom. From left to right: original partial-ring MLEM reconstruction, corrected image using U-Net, corrected image using the proposed INR, and reference ground-truth image obtained with the full-ring scan.

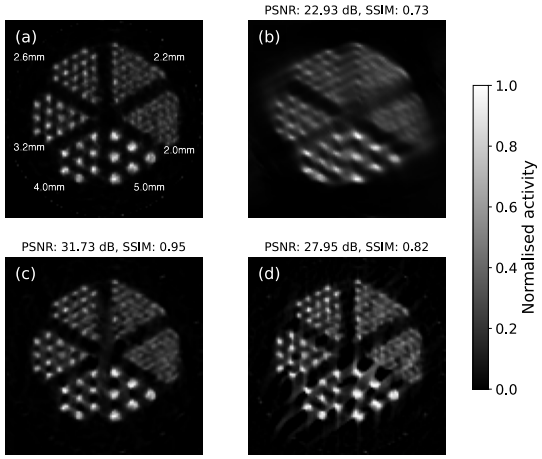

Figure 3: Results of the INR learning in representing the MC simulated Derenzo phantom.(a) Ground truth full-ring image, annotated with sphere diameters.(b) Partial-ring image.(c) Prior initialized INR corrected image and (d) INR corrected image without a prior.

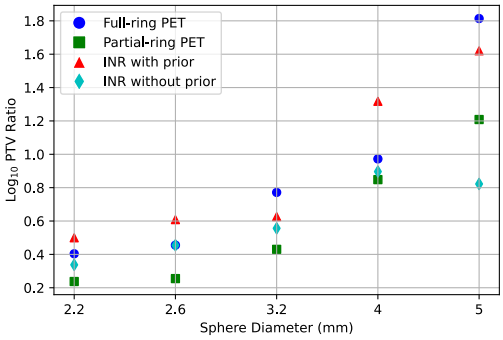

Figure 4: Peak-to-valley(PTV) ratio comparison amongst the four reconstructed Derenzo phantom images shown in Figure 3 for different sphere diameters.

compared to the initial partial-ring reconstruction. INR achieved a PSNR of 35.49 dB and an SSIM of 0.98 compared to the ground-truth full-ring PET image. Line profiles also illustrate INR's ability to recover intensities comparable to the ground truth full-ring image.

4 Discussion

This study presents an INR-based approach for partial-ring PET image correction. Unlike traditional data-driven deep learning methods that often suffer from overfitting issues and require extensive datasets, the proposed INR model does not require any external dataset but only uses the acquired partial-ring image for model training. This patient-specific nature of INR enables optimized imaging for each individual scan.

The efficiency of INR learning is seen by its faster training times compared to the 2D U-Net model. Additionally, the size of the model is dependent on the complexity of the signal rather than the discrete voxel grid size.

Our evaluation across three distinct datasets (analytically simulated brain phantom data, Monte Carlo simulated data, and phantom measurement data) demonstrates its robustness. For the digital brain phantom data, the INR model consistently achieved high PSNR and SSIM values, comparable or superior to U-Net, but with the added advantage of reduced training time. The model's ability to recover signal in artificially-inserted lesions in the brain phantom dataset, as seen in figure 2, illustrates its effectiveness in capturing structural changes and recovering missing signals. Inclusion of scanner effects in the dataset further extends the application of the method to realistic imaging scenarios. The performance improves with prior initialization of the INR model, especially in intensity prediction and separation of individual spheres in the Derenzo phantom. Similar performance was observed in measured data, reinforcing the application to different scenarios. Furthermore, the proposed network architecture can significantly benefit longitudinal PET studies. For in-

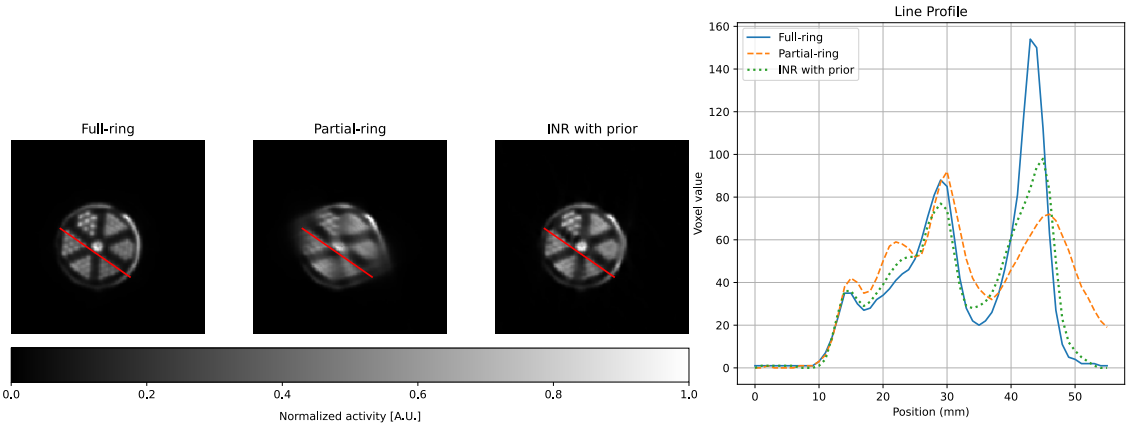

Figure 5: Depiction of full-ring, partial-ring and INR reconstructed images for the experimental hot-rod phantom. Line profile through the red line indicated in the three images is shown in the fourth column.

stance, in fractionated treatments where a new PET scan is required for verification or adaptation, the model trained during the first fraction can be reused for subsequent fractions. This not only saves inference time but also utilizes prior information to fine-tune important features.

Despite its advantages, the model has only been tested for phantom studies, due to the constraints of the PETITION PET scanner. This highlights the need for further validation with measured patient data. Future work will explore the model's performance in patient imaging and its extendibility to higher dimensionalities, such as 3D PET imaging.

5 Conclusion

This study demonstrates an INR-based approach for PET image correction, offering significant advantages in terms of efficiency and image quality. The model has been evaluated for partial-ring PET scanners without requiring a large training dataset. This approach helps in the development of further dedicated limited angle PET scanners or tomographs for varying applications.

Acknowledgements

This project was supported by the Swiss National Science Foundation, Grant No. CRSII5 189969.

References

[1] R. D. Badawi, H. Shi, P. Hu, et al. "First human imaging studies with the EXPLORER total-body PET scanner". *Journal of Nuclear Medicine* 60.3 (2019), pp. 299–303.

[2] M. Watanabe, K. Shimizu, T. Omura, et al. "A new high-resolution PET scanner dedicated to brain research". *IEEE Transactions on Nuclear Science* 49.3 (2002), pp. 634–639.

[3] S. Surti and J. S. Karp. "Design considerations for a limited angle, dedicated breast, TOF PET scanner". *Physics in Medicine & Biology* 53.11 (2008), p. 2911.

[4] M. G. Bisogni, A. Attili, G. Battistoni, et al. "INSIDE in-beam positron emission tomography system for particle range monitoring in hadrontherapy". *Journal of medical imaging* 4.1 (2017), pp. 011005–011005.

[5] H. W. De Jong, R. Boellaard, C. Knoess, et al. "Correction methods for missing data in sinograms of the HRRT PET scanner". *IEEE Transactions on Nuclear Science* 50.5 (2003), pp. 1452–1456.

[6] S. M. Valiollahzadeh, T. Chang, J. W. Clark, et al. "Image recovery in pet scanners with partial detector rings using compressive sensing". *2012 IEEE Nuclear Science Symposium and Medical Imaging Conference Record (NSS/MIC)*. IEEE. 2012, pp. 3036–3039.

[7] M. Burger, J. Müller, E. Papoutsellis, et al. "Total variation regularization in measurement and image space for PET reconstruction". *Inverse Problems* 30.10 (2014), p. 105003.

[8] V. Sitzmann, J. Martel, A. Bergman, et al. "Implicit neural representations with periodic activation functions". *Advances in neural information processing systems* 33 (2020), pp. 7462–7473.

[9] L. Shen, J. Pauly, and L. Xing. "NeRP: implicit neural representation learning with prior embedding for sparsely sampled image reconstruction". *IEEE Transactions on Neural Networks and Learning Systems* (2022).

[10] C. E. Ritzer, V. Commichau, J. Flock, et al. "The PETITION Project-Initial Monte-Carlo Simulations" (2021).

[11] B. Aubert-Broche, M. Griffin, G. B. Pike, et al. "Twenty new digital brain phantoms for creation of validation image data bases". *IEEE transactions on medical imaging* 25.11 (2006), pp. 1410–1416.

[12] C. Da Costa-Luis. "BrainWeb-based multimodal models of 20 normal brains". *Jul-2019 [Online]. Available: https://doi.org/10.5281/zenodo* 3269888 (2019).

[13] S. Jan, G. Santin, D. Strul, et al. "GATE: a simulation toolkit for PET and SPECT". *Physics in Medicine & Biology* 49.19 (2004), p. 4543.

[14] C.-C. Liu and H.-M. Huang. "Partial-ring PET image restoration using a deep learning based method". *Physics in Medicine & Biology* 64.22 (2019), p. 225014.